$c(2\times2)$S/Cr(001) surface and near-surface structure determined using angle-resolved photoemission extended fine structure

L. J. Terminello, X. S. Zhang,* Z. Q. Huang, S. Kim, A. E. Schach von Wittenau, K. T. Leung,† and D. A. Shirley
Department of Chemistry, University of California, Berkeley, California 94720
and Materials and Chemical Sciences Division, Lawrence Berkeley Laboratory, 1 Cyclotron Road, Berkeley, California 94720
(Received 1 February 1988)

We report the surface and near-surface structure of $c(2\times2)$S/Cr(001) determined from angle-resolved photoemission extended fine structure (ARPEFS). The sulfur 1*s* photoemission partial cross section was measured in the [001] and [011] emission directions, yielding fine-structure amplitudes up to 50–70%. Qualitative results were obtained from Fourier transforms of the ARPEFS, revealing geometrical information beyond 10-Å path-length difference from the photoemitter. Structural parameters were determined with greater precision by comparing the Fourier-filtered data to multiple-scattering spherical-wave calculations. The high directional sensitivity of ARPEFS was apparent in the analysis of normal [001] and off-normal [011] emission-direction data. Sulfur adsorbs in the fourfold hollow site 1.17 Å above the first chromium layer, and the first- to second-layer chromium distance *contracts* to 1.31 Å, 8% less than the 1.44-Å bulk value. Analysis of the near-surface contribution to ARPEFS showed that deeper layers essentially retain the bulk separation.

I. INTRODUCTION

Photoelectron diffraction as a probe of surface structure was originally suggested by Liebsch[1,2] and was observed by three groups[3–5] in different experimental arrangements. Among these, the angle-selected, variable-energy form of photoelectron diffraction has been applied extensively in this laboratory. Initially the adsorbate core-level photoelectron peak intensity was studied along the crystal normal, over a limited energy range (typically $\approx$100–150 eV), and compared to multiple-scattering calculations derived from low-energy electron-diffraction (LEED) theory.[6] The term "normal photoelectron diffraction" (NPD) was used to describe this approach. With the realization[7] that NPD curves could be Fourier transformed to yield peaks corresponding to distances, our emphasis has shifted to recognize the similarities between variable-energy photoelectron diffraction and extended x-ray-absorption fine structure (EXAFS),[8] stimulated by the qualitative success of a single-scattering cluster model.[9] The name angle-resolved photoemission extended fine structure (ARPEFS) was coined to distinguish this new approach. ARPEFS is more general than NPD, while in a sense it includes NPD. In ARPEFS the angle is fixed but not necessarily normal to the surface, and the data range is as long as practicable, usually $\approx$50–500 eV above threshold. Several adsorbate geometries have been determined by ARPEFS.[10–14]

A reasonably complete approximate understanding of the applicability and limitations of ARPEFS as a structural method have emerged from this earlier work. For example, Fourier transform analysis provides definitive site-geometry information, but back-transformation analysis may not be feasible. Similarly, a simple single-scattering plane-wave model usually simulates ARPEFS data semiquantitatively, but an accurate structural analysis requires a more quantitative multiple-scattering spherical-wave (MSSW) model.[15] With a MSSW-level analysis effects as subtle as substrate reconstruction could be characterized. Nevertheless some rather basic issues were still in need of clarification. Of particular interest is the extent to which thermal effects (large mean-square relative atomic displacements) in the substrate lattice reduce the amount of structural information present in the fine structure. A related issue is the depth to which ARPEFS can probe, i.e., from how many atomic layers is an ARPEFS signal derived?

We have studied the system $c(2\times2)$S/Cr(001) to provide experimental insight into these questions, among other reasons. The stiffness of the chromium lattice makes this element a strong candidate for controlled studies of phonon-induced effects. Study of the $c(2\times2)$S/Cr(001) system is complementary to a study of $c(2\times2)$S/Fe(001) presently underway in our laboratory,[16] as well as to recent work on the oxidation of the Cr(001) surface[17,18] and recent work on the magnetic properties of this surface.[19,20]

This paper is organized into five sections. Section II provides details of collecting the photoemission spectra that constitute ARPEFS; Sec. III describes data-reduction procedures and the two forms of analysis we perform to extract structural information: Fourier and multiple-scattering analysis. Section IV discusses the results and error analysis, and the overall procedure is summarized in Sec. V.

II. EXPERIMENT

A. Sample preparation

The $c(2\times2)$ sulfur overlayer was prepared on a clean Cr(001) surface. The chromium substrate was cut and

polished from a single-crystal rod and was oriented to within $\pm 1°$ of the (001) surface by Laue backscattering. This $5\times5\times3$ mm^3 sample was attached with tantalum strips to a 0.010-in. tantalum plate to allow electron beam heating from behind. The sample holder was mounted on a three-axis manipulator that permitted rotation about the vertical axis and azimuthal alignment of the crystal surface.

Cleaning the chromium surface has long been recognized as a difficult task. It was once believed that the clean Cr(001) surface reconstructed to give a $c(2\times2)$ low-energy electron-diffraction (LEED) pattern. Subsequent[21] studies showed that residual surface contaminants caused the apparent reconstruction and that a truly clean Cr(001) face gives a sharp (1×1), low-background LEED pattern. This has been confirmed by ultraviolet photoelectron spectroscopy[19] and by high-resolution electron energy loss spectroscopy.[17] The Cr(001) surface was cleaned by Ar^+ sputtering at energies of 1000 eV followed by 1120 K annealing for several minutes. Temperatures were measured by a Chromel-Alumel thermocouple attached near the sample; an infrared pyrometer calibrated the thermocouple giving an estimated 20° accuracy for temperature measurements. Sputtering was sufficient to remove surface contaminants but subsequent annealing segregated bulk impurities to the surface. Because the sample had been cleaned for an earlier[22] experiment, the majority of the bulk impurities were absent and only a few days of sputter-anneal cycles were necessary. Surface cleanliness was verified by Auger-electron spectroscopy (AES) and LEED. AES showed no carbon, nitrogen, oxygen, or sulfur contamination, although the oxygen Auger signal was difficult to quantify because of its overlap with the chromium signal.

LEED provides an additional measure of surface integrity since the sharp (1×1) pattern of the clean surface is easily converted to a sharp $c(2\times2)$ by small amounts of impurities. Foord, Reed, and Lambert[23] have reported that an intense $c(2\times2)$ LEED pattern is present after annealing the Cr(001) surface in the presence of ambient contaminants. Reed, Lambert, and Foord[24] have determined that the impurity coverage of $\theta\approx0.2$ monolayers gives sharp $c(2\times2)$ LEED patterns, and they interpret this as $c(2\times2)$ impurity island formation which gives rise to intense fractional order beams. This would leave large, clean (1×1) areas on the surface. Because of this, the sharp $c(2\times2)$ LEED pattern is somewhat misleading as an indication of surface coverage.

There have been relatively few reports of sulfur overlayer studies on chromium. Gewinner[18] reported that S/Cr(001) forms a $c(2\times2)$ overlayer by either H_2S dosing followed by a 300 °C anneal or diffusion from the bulk. Our sulfur overlayers were prepared by dosing the clean (1×1) Cr(001) surface with H_2S from an effusive-beam gas doser. This produced a diffuse $c(2\times2)$ LEED pattern. Dosing was followed by a 700-K anneal for 5 min to desorb any hydrogen, yet leaving behind sulfur. The resulting LEED pattern was a sharp $c(2\times2)$ with no background. The sulfur coverage was monitored by AES and showed some change in the S (152 eV) to Cr (529 eV) Auger signal ratio before and after annealing. After ambient contaminants (carbon and oxygen from CO) would coadsorb onto the surface, we could reanneal the sample with no change in the LEED pattern or the sulfur-chromium Auger emission ratio. This recovered the initial S/Cr surface without any apparent diffusion of the sulfur into the bulk. By monitoring the Auger signal for sulfur and chromium and by examining LEED, we can conclude that the $c(2\times2)$S/Cr(001) surface that we studied by ARPEFS had $\lesssim0.5$ monolayer of sulfur adsorbed.

B. Equipment

Sulfur 1s ARPEFS was taken at the Stanford Synchrotron Radiation Laboratory on Beamline III-3 using the jumbo double-crystal monochromator.[25] Photoemission spectra were taken in the 50–550-eV kinetic energy range using 2525–3025-eV photons. The monochromator used two Ge(111) crystals capable of producing the necessary photons for this experiment and with $\gtrsim98\%$ polarization in the horizontal plane.

Photoelectrons were collected with a hemispherical electrostatic analyzer that was described previously.[26] Under operating conditions of 160 eV pass energy the analyzer's energy resolution is ≈1 eV and angular resolution of the input lens is $\pm3°$. The experimental chamber containing the angle-resolving analyzer also has a four-grid LEED system capable of doing LEED and AES; an ion gun and effusive beam gas inlet are also present for sample preparation.

Typical pressures of the experimental chamber during the ARPEFS measurements were 2×10^{-10} torr. Because of the sensitivity of the S/Cr surface to ambient contaminants, the sample would be reannealed every 6–9 h during data collection. By staggering this reannealing point throughout the experiment, we were able to show that this procedure of maintaining sample integrity had no effect on the ARPEFS measurements within the limits of our photoemission intensity measurements ($\approx2\%$).

C. Data collection and reduction

Angle-resolved photoemission spectra were taken in two geometries that take advantage of the directional sensitivity of ARPEFS. It has been speculated[18] that sulfur adsorbs onto Cr(001) into the fourfold-hollow site, as do most adsorbates. Our electron emission geometries were selected to confirm this adsorption site or to identify another likely site prior to determining the surface structure. Figure 1 illustrates the $c(2\times2)$S/Cr(001) surface with emission and photon polarization directions used in the experiment.

The [001] emission direction was selected both because of its high symmetry and because the back scattering that contributes strongly to the ARPEFS would originate from the bulk and thereby highlight the interlayer distances in our final result. Photoemission along the surface normal would reveal the interlayer spacing information better than any other experimental geometry. For this direction the photon polarization vector, $\hat{\epsilon}_{[001]}$ was aligned 35° off-normal directed towards [011]. For sensitivity to structural parameters parallel to the surface an off-normal emission direction was also selected. The

[011] emission direction would help differentiate the fourfold-adsorption site from any other because the proximity of backscatterers in the fourfold hollow would give a unique interference pattern for the [011] direction. This would provide the sensitivity to observe any second-layer substrate corrugation. For this experimental geometry the polarization vector $\hat{\epsilon}_{[011]}$ was parallel to the [011] emission direction. These emission directions were determined by He-Ne laser autocollimation referring to the experimental chamber viewports. Photon polarization vectors were referred to the experimental chamber in a similar manner. Accuracies in these measurements were estimated at $\pm 2°-3°$ and are due to the laser spot size, chamber viewport alignment, and Cr surface smoothness.

Sulfur 1*s* photoemission spectra were taken in constant wave-vector increments to give a regularly spaced ARPEFS curve. For the [001] direction the spectra were taken in 0.1-Å^{-1} increments in the energy range specified above; off-normal data were taken in 0.08-Å^{-1} increments. Three series of spectra were taken for the normal emission data on separately prepared samples to verify reproducibility. Each series of 80–100 photoemission spectra constitute a given data set whose density is important for Fourier transformation and information extraction.

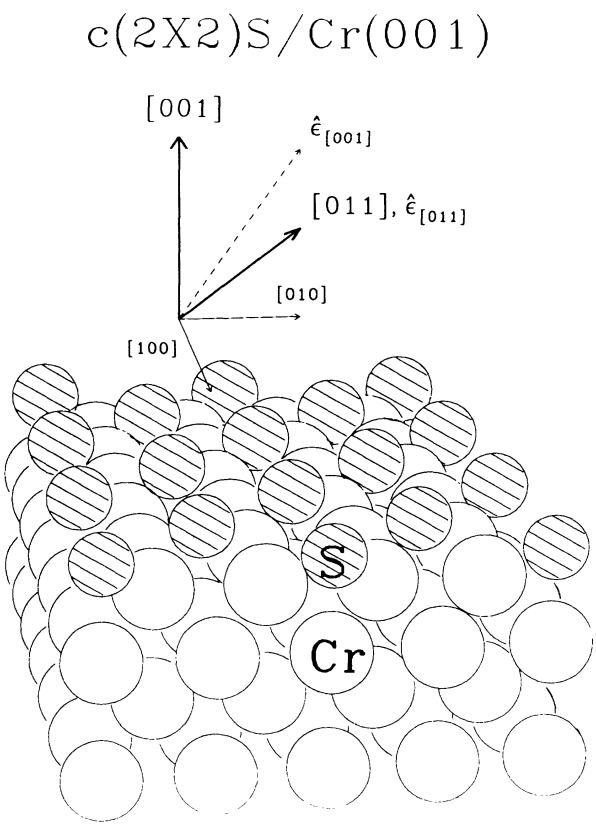

FIG. 1. Adsorbate-substrate model with experimental geometries. This depicts the $c(2\times2)$ overlayer of sulfur (shaded atoms) on the (001) face of a chromium single crystal. The emission directions (bold vectors) described in the text are labeled [001] and [011]. Photon polarization vectors (dashed vectors) associated with each of these experimental geometries are labeled $\hat{\epsilon}_{[001]}$ and $\hat{\epsilon}_{[011]}$, respectively.

To generate the photoemission partial cross section, it is necessary to normalize each photoemission spectrum to compensate for photon flux inhomogeneities and the analyzer transmission function. The intensity normalization and extraction procedure has been described previously.[10,12] For this experiment the 40–500 eV electron emission spectrum was taken at a photon energy of 2400 eV for each curve; these provide a background template against which we normalized individual photoemission spectra for each direction.

Photoemission from metals has been described by Doniach and Šunjić.[27] The asymmetric line shape they describe includes the core photopeak, plus core photoelectrons that have inelastically scattered from the conduction electrons, and background electrons that arise from other photoemission processes in the sample. Earlier ARPEFS experiments[10,14] have extracted the photoemission intensities that constitute ARPEFS by modeling the core photopeak with a Gaussian, the inelastic tail by a Gaussian-broadened step function, and the background electrons by the empirically determined background template. Barton *et al.*[10] have indicated that using a Gaussian to model the photopeak oversimplified the description of the photoemission intensity because some additional broadening was not included. We have attempted to remedy this by modeling the core photopeak with a Voigt (Gaussian convoluted with a Lorentzian) function.[28] This enabled us to model lifetime broadening present in the photoemission peak in addition to monochromator and analyzer contributions to the line shape. Krause and Oliver[29] have calculated the natural *K*-shell linewidths of various elements, a value of 0.59 eV (FWHM) for sulfur. Using this as a starting point, we least-squares fitted sulfur 1*s* photoemission spectra with a Voigt, a Gaussian convoluted with a step function (a *G* step), and the background template.

Photoemission peaks were fitted throughout the data range. Best fits were obtained for Lorentzian widths of approximately 0.8 eV FWHM. Because this width was both close to the calculated value of 0.59 eV and effectively constant throughout the data range, we concluded that a Voigt function is justified. Next, we constrained the widths of the *G* step and the Gaussian portion of the Voigt to be equal and kept the Lorentzian portion of the Voigt width fixed at 0.8 eV. This left the Voigt area, mean, Gaussian width of the Voigt, the *G*-step area, and background template proportionality factor as the only parameters varied in these fits. We emphasize that using a Voigt function to model the photopeak does not add another parameter simply to improve the fits. Rather, we have modeled the lifetime contribution to the sulfur 1*s* line shape.

Once the photoemission spectra have been modeled by these various parameters the ARPEFS intensity curves were constructed. The Voigt area obtained in the fitting procedure is the photoemission intensity of interest. Our $I_t(E)$ is constructed by plotting the Voigt peak area as a function of the Voigt mean, using the background template proportionality factor to normalize each photoemis-

sion spectrum. Each normalized curve is then multiplied by the kinetic energy to compensate for the analyzer transmission function. The total intensity $I_t(E)$ can be expressed as:

$$I_t(E)=[\chi(E)+1]I_0(E)\ , \tag{1}$$

where $I_0(E)$ is the slowly varying, atomiclike contribution to the total intensity and $\chi(E)$ is the rapidly oscillating part—the fine structure we seek. $\chi(E)$ is obtained from the total intensity $I_t(E)$ and its extraction is illustrated by rearranging Eq. (1)

$$\chi(E)=[I_t(E)/I_0(E)]-1\ .$$

The selection of a suitable $I_0(E)$ is contingent on the results of subsequent Fourier analysis that give minimal intensity to the Fourier amplitude at zero. The optimal results for the two emission directions were obtained by using a cubic polynomial to model $I_0(E)$. The $\chi(E)$ curves obtained in this manner are pictured in Figs. 2 and 3 for the [001] and [011] directions, respectively; note the large amplitude (50–70 %) of the [001] data.

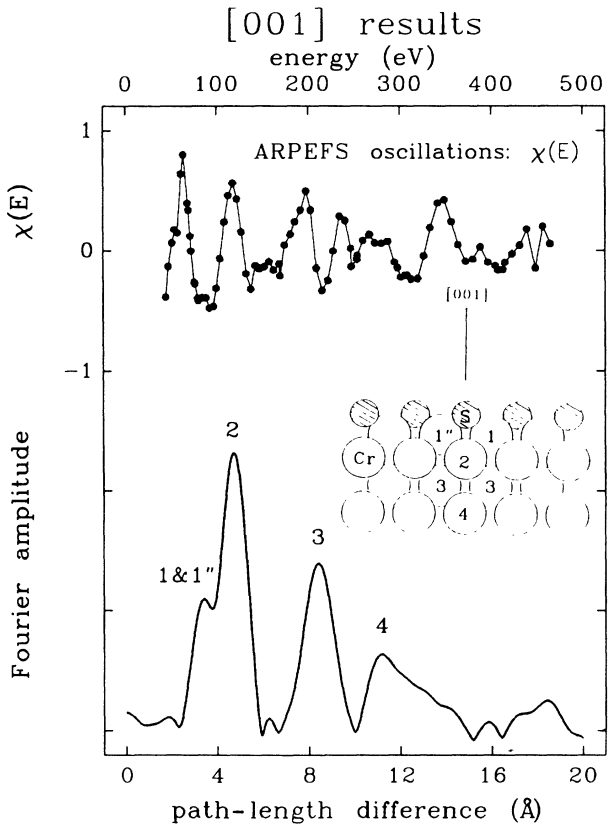

FIG. 2. $\chi(E)$ and Fourier transform: [001] data. This shows the $\chi(E)$ for the normal emission data (upper portion) taken directly from $I_t(E)$ by utilizing Eq. (1). Each data point (solid dot) represents the contribution to $\chi(E)$ from a single photoemission spectrum. The Fourier transform of the $\chi(E)$ after it has been converted to $\chi(k)$ is pictured below it. Each numbered peak is associated with scattering path-length differences for the similarly numbered atoms in the side-view model. Each path length is measured from the photoemitter S.

III. DATA ANALYSIS

Structural information is extracted by two methods from the extended fine structure. Fourier transformation of the ARPEFS yields elastic-scattering, path-length difference information and gives a semiquantitative result for geometrical parameters that aid in adsorption-site identification. Results with higher precision are obtained by comparing the experimental curves to multiple-scattering spherical-wave calculations. Analysis procedures for this experiment follow.

A. Fourier analysis

The single-scattering model of ARPEFS (Ref. 8) illustrates the cosinusoidal dependance of the oscillations and can be written as

$$\chi(k)=2\sum_j \frac{\cos\beta_j}{\cos\gamma}\frac{|f(\theta_j)|}{r_j}\cos[kr_j(1-\cos\theta_j)+\phi_j] \times e^{-\Delta R_j/\lambda}e^{-\sigma_j^2(1-\cos\theta_j)k^2}\ , \tag{2}$$

where r_j is the distance from the photoemitter to the jth scattering atom and θ_j is the scattering angle at the jth atom. γ is the angle between the emission direction and the photon polarization vector while β_j is the angle between the photon polarization vector and the vector con-

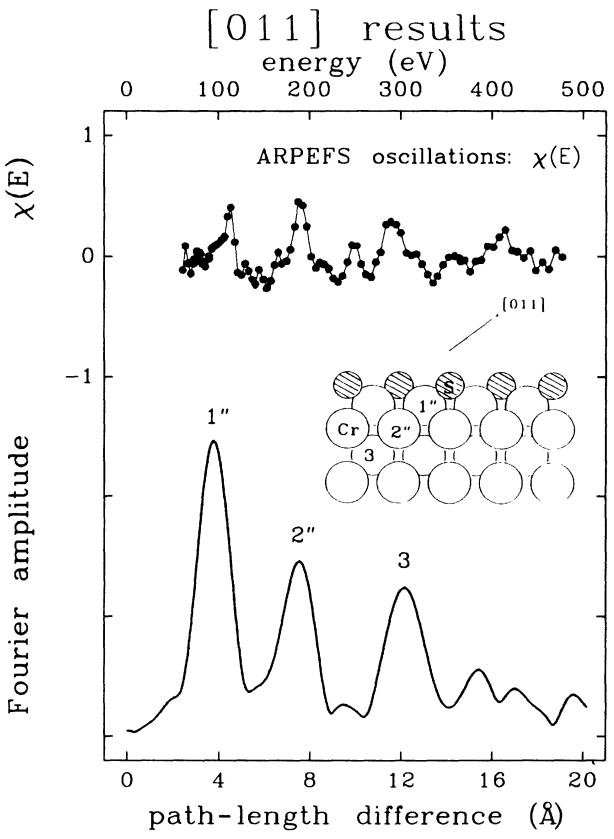

FIG. 3. $\chi(E)$ and Fourier transform: [011] data. The same information as Fig. 2, but for the [011] emission data. Note the directional sensitivity of the data and the high frequency of the oscillations.

necting the photoemitter and the jth scattering atom. $f(\theta_j)$ is the k-dependant scattering factor for a given scattering angle θ_j and has been factored into a magnitude $|f(\theta_j)|$ and phase ϕ_j. Attenuation of the ARPEFS signal due to inelastic losses are modeled by an electron mean-free path λ while the thermal averaging is included in a Debye-Waller term where σ_j^2 is the mean-square relative displacement of the jth scattering atom. The Fourier transformation of this function would give amplitudes at values near $r_j(1-\cos\theta_j)$ for each jth scattering atom. The value $r_j(1-\cos\theta_j)$ represents the scattering path-length difference and is easily recognized from the Fourier spectrum for short path-length scattering conditions.

The initial steps in Fourier analyzing the ARPEFS is to convert the energy-dependent fine structure $\chi(E)$ to a function of wave vectors (Å^{-1}) which lends itself to Fourier transformation. We perform this conversion by using the de Broglie relationship:

$$k=\hbar^{-1}[2m_e(E+V_0)]^{1/2}, \tag{3}$$

where E is the photoelectron kinetic energy measured outside the solid, m_e is the electron rest mass, and V_0 is the inner potential of the solid. The exact value of V_0 is unknown and is dependent on the solid and energy. We treated V_0 as an adjustable parameter in the analysis and have determined a value of 10.5 eV to be optimal. Other ARPEFS experiments on Ni[10,11] have used similar values of V_0.

Each $\chi(k)$ is spline interpolated onto an even mesh and then windowed[30] prior to Fourier transformation. Windowing compensates for the finite data range of $\chi(k)$, thereby suppressing additional features in the Fourier amplitude spectrum (ringing). We multiply the data with a Gaussian window function having an area of 1, a mean set at the center of the data range, and a width equal to $\frac{5}{8}$ the $\chi(k)$ range in Å^{-1}. This tapers the $\chi(k)$ data, alleviating any ringing problem while minimizing the loss of information. The fast Fourier transform[31] is applied to the data, giving an amplitude spectrum peaked near various scattering path-length differences. The $\chi(k)$ and Fourier transforms for the [001] and [011] emission-direction data are pictured in Figs. 2 and 3, respectively. In each case strong features are present at path lengths greater than 10 Å, indicating that scattering from near-surface atoms makes a sizable contribution to the ARPEFS signal. While previous ARPEFS experiments yielded path-length information out to 10 Å, we are confident our sensitivity goes beyond 10 Å because of the relative intensity of the features at longer path-length differences. Reproducibility of the large path-length Fourier features in the normal emission data provided additional proof.

Various forms of the fitting functions for $I_0(E)$ were tried until a Fourier spectrum of zero amplitude at zero path-length difference was obtained. The procedure of minimizing the amplitude at zero path-length difference may introduce some error into the analysis because short path lengths due to ARPEFS may be deleted from the data by unintentional removal of low-frequency information from $\chi(E)$. With the single-scattering, plane-wave model of ARPEFS described by Eq. (2), we can attempt to assign each peak in the Fourier transforms to one or more scattering atoms. While this is adequate for the first few features in the Fourier spectrum because they are generated by atoms near the photoemitter, long path-length features are not as easily assigned. The normal and [011] emission data are interpreted this way.

The initial step of the Fourier analysis is the determination of the adsorption site. Previous work on chromium[18] concluded that sulfur most likely adsorbs on the (001) face in the fourfold hollow generated by four neighboring first-layer atoms; this symmetry agrees with the LEED pattern. Other sites considered are the "atop" site where sulfur adsorbs directly above a first-layer Cr and a "bridge" site where an S atom may sit above and between two adjacent first-layer chromium atoms. Because the largest ARPEFS amplitudes are usually generated by direct backscatterers, we may qualitatively determine the sulfur adsorption site from the Fourier spectra.

Examination of the normal emission Fourier transform shows a large peak at 4.7 Å that is most likely due to the presence of a backscatterer directly below the photoemitter. Assuming the bridge site, the most likely geometry would have the S$\approx$2.1 Å above two adjacent first-layer chromium atoms. This site would not suitably explain the shoulder at 3.2 Å on the left of the main peak while nominally justifying the main feature at 4.7 Å. The other two possibilities, atop and fourfold hollow, both have a chromium atom directly below the sulfur atom. For the atop site, the sulfur would be situated about 2.4–2.5 Å above a first-layer Cr atom. This gives a rather unusual coordination to a sulfur atom, making this site marginally credible, at best.

The [011] emission data provide conclusive evidence for selecting the fourfold site. Should the sulfur be adsorbed in an atop site, the nearest backscatterer for the off-normal emission would be 3.8 Å away (an adjacent first-layer Cr atom), giving a peak in the Fourier transform near 6-Å path-length difference, which is not present. The Cr atom directly below the photoemitter would then have a scattering path length of 4.0 Å, close to the 3.8-Å feature, but too intense for such a weak scattering condition (135° scattering). The strength of the 3.8-Å feature in the [011] transform cannot be easily explained using the atop-site model. This large feature can easily be understood using a fourfold-site model because the proximity of the first-layer near neighbors would generate this peak in the [011] transform. This qualitative argument is substantiated by the multiple-scattering spherical-wave analysis that follows and serves as a basis from which to begin the detailed structural interpretation.

Scattering from the Cr second-layer atom directly below the sulfur would be assigned to the largest feature (peak 2) in the [001] data at a path-length difference of 4.7 Å. The strength of this peak illustrates the importance of backscattering (180°) in the ARPEFS spectrum. While strict adherence to the single-scattering model described in Eq. (2) would reduce interpretation of the ARPEFS Fourier spectrum to an exercise in geometry, in

fact multiple-scattering effects also contribute. It has been shown[10,11] that for this 180° scattering event, forward scattering and focusing through the photoemitter contributes, and the multiple-scattering component of the ARPEFS structure is actually comparable to the single-scattering portion. Because the additional phase shift incurred through forward scattering is small, the multiple-scattering and single-scattering components have similar effective path lengths for this scattering geometry.

The shoulder on the left of the main feature at 3.2 Å arises from the four nearest-neighbor Cr atoms located in the first layer of the substrate. All four contribute to the ARPEFS with the same path-length difference but not with the same amplitude. The sulfur 1*s* photoelectron is emitted as a *p*-like wave whose symmetry axis is parallel to the photon polarization vector. The polarization vector $\hat{\epsilon}_{[001]}$ is 35° down from the [001] emission angle, causing the S photoelectron to propagate unsymmetrically with respect to the surface normal. Therefore, the two Cr atoms behind the sulfur lying along the photon polarization direction contribute more than the two which lie near the *p*-wave node—effectively making two pairs of nonequivalent scatterers from the four nearest-neighbor, symmetry-equivalent Cr atoms.

The third feature, at 8.4 Å in the [001] Fourier spectrum, is largely due to third-layer Cr atoms that lie directly below the four first-layer nearest-neighbor Cr atoms. Features beyond the 8.4-Å peak have substantial amplitude and can be nominally assigned to scattering from (one or a few) particular atoms. The peak at 11.2 Å can be attributed in part to scattering from the *fourth*-layer Cr atom located directly below the S photoemitter. One should be cautious regarding such assignment, because many scatterers are present. Also, multiple scattering is important in understanding the contribution of the fourth-layer Cr atoms to the ARPEFS. Barton *et al.*[10,32] have shown that multiple scattering is largely forward focusing and has little effect on determining the path-length difference; this may explain why we see such large contribution from the fourth layer. Various multiple-scattering propagation schemes involving the second-layer chromium atom or the photoemitter itself can contribute to the ARPEFS at effectively the same path-length difference, giving rise to the surprisingly large Fourier amplitude for such a distant scatterer. Peak assignments beyond 11.2 Å will not be attempted, because of the difficulty of assigning a unique set of scattering events to a given feature. Multiple scattering is obviously essential when interpreting these higher frequency, low-amplitude features.

A similar analysis of the [011] emission data was made. The emission direction and photon polarization vector are parallel in this experimental geometry. In this configuration the photoelectron to be backscattered propagates directly into the substrate at a 45° angle with respect to the normal. This lateral propagation into the bulk illuminates the substrate atoms below and to the sides of the photoemitter, giving greater lateral sensitivity parallel to the surface than the normal emission data. The first feature at 3.8 Å in the [011] Fourier spectrum in Fig. 3 arises mainly from two of the first-layer nearest-neighbor Cr atoms: the other two nearest-neighbor atoms, which do not contribute much to the total signal, lie near the photoemission *p*-wave node. The second large feature at 7.6 Å is generated largely by a second-layer Cr atom adjacent to one directly below the photoemitter. This scatterer has no sulfur adsorbed above it and is therefore in a chemically different environment than a second-layer chromium atom *with* a sulfur directly above. This illustrates the directional sensitivity of ARPEFS and how it can be used to illuminate different second-layer substrate atoms to uncover detailed reconstruction information.

Backtransform techniques have been applied to ARPEFS data in previous experiments.[11] In these studies a single Fourier transform feature was isolated and then backtransformed to yield amplitude and phase information. The phase of the backtransform would contain path-length difference information plus the scattering phase-shift ϕ_j described in Eq. (2). Unfortunately the effective phase shift is due to single *and* multiple scattering, thereby obfuscating the path-length difference information. We shall therefore forego the backtransform analysis of our ARPEFS and make quantitative structure determinations by multiple-scattering analysis.

B. Multiple-scattering analysis

Fourier analysis alone provides useful information about the major features in the amplitude spectrum, but it is limited in its ability to determine subtle structural changes. For this we compare the experimental $\chi(k)$ to simulated data based on a given geometrical configuration. This approach allows more quantitative results to be obtained from the experimental data because smaller features, which are difficult to interpret by Fourier analysis, can be modeled by the calculations.

We compared our experimental ARPEFS to multiple-scattering, spherical-wave (MSSW) calculations based on a model developed by Barton, Robey, and Shirley.[32] They have shown that a single-scattering plane-wave model[9] is insufficient to describe the extended fine structure completely. The MSSW theory takes as input the adsorbate-substrate geometry, Debye temperature, mean-free path parameter, emission and polarization directions, detector aperture size, and atomic partial-wave phase shifts. The parameter most sensitive to the theory is the crystal geometry.

The chromium phase shifts were calculated using a modified program of Pendry.[33] The Cr potential used in this program was obtained from the local-density approximation calculations of Moruzzi, Janak, and Williams,[34] while sulfur phase shifts were calculated previously.[11] The bulk Debye temperature was set at 470 K and the surface Cr Debye temperature at 332 K. This assumed that the surface Cr atoms would have a mean-square relative displacement (MSRD) twice that of the bulk. The sulfur Debye temperature was estimated to be 423 K and was arrived at by using a mass substitution of sulfur for chromium.[32] Recent reports of anisotropies in surface MSRD draw contradictory conclusions. Roubin *et al.*[35] have determined by surface extended x-ray-absorption

fine structure (SEXAFS) that the surface MSRD in the direction perpendicular to the surface is 1.25 times greater than in the surface plane for Co/Cu(111). Sette *et al.*[36] have shown the opposite effect on the $c(2\times2)$Cl/Cu(001) system, also using SEXAFS. They report that the surface-parallel vibrational amplitudes are twice as great as the surface-perpendicular ones. This apparent discrepancy may arise from differences in the adsorbate-substrate interaction between the two systems. We have attempted to observe any anisotropy at the surface by varying the surface parallel and perpendicular MSRD within our model.

The mean-free path was modeled by setting a proportionality factor c in the exponential damping term $e^{-r/\lambda}$, where $\lambda=ck$. We used a value of 0.75 for c, which is similar to values used for Ni ARPEFS experiments. Allen, Tucker, and Wild[37] have reported an empirically determined mean-free path of 12 Å for chromium from Cr $2p$ photoemission at energies of 574 and 538 eV. Selection of a suitable value for c is coupled to the choice of Debye temperatures and their anisotropies parallel and perpendicular to the surface.

The theory allows us to specify the cluster size for the scattering calculations. Cluster sizes were selected with ≤ 10 Å radius so that any distant, near-surface contribution to the ARPEFS would be included. The extended range of strong amplitudes in the Fourier transform beyond 10-Å path-length difference necessitated this large cluster size.

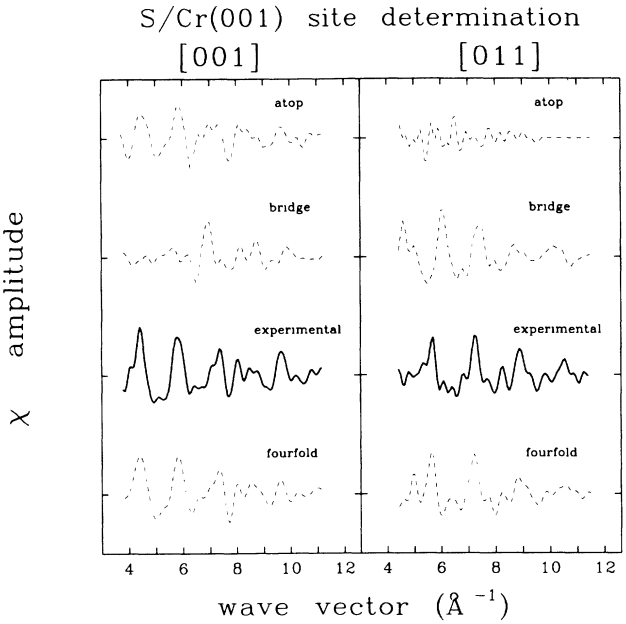

FIG. 4. Site selection using MSSW curves compared to experiment. Comparison of experimental curves (solid lines), to the MSSW theory curves (dashed lines) for three adsorption sites: atop, bridge, and fourfold. The fourfold site compares favorably in both the [001] emission set (left panel) and the [011] set (right panel) while the other sites do not.

1. Site determination

Fourier analysis provides strong arguments for adsorption site selection, but a careful comparison of MSSW calculations with experiment can give conclusive evidence for choosing the fourfold hollow as the adsorption site and yield structural parameters. A series of calculations was performed on $c(2\times2)$S/Cr(001) that varied the layer spacings, using three adsorption site models. Figure 4 shows the comparison of the normal and [011] emission data with the calculated χ curves for the atop, bridge, and fourfold sites. Each calculated curve represents the best fit to the experimental results for that adsorption site, in which the first and second substrate layer spacings were varied. By visual comparison we can see that the atop and fourfold sites are both similar to the experimental results with the latter being somewhat closer. The weaker bridge site extended fine structure is out of phase with the [001] emission data, thus easily eliminating this site choice. The atop and fourfold site seem quite similar because each model contains a backscatterer directly below the photoemitter which contributes strongly to the total ARPEFS.

From the off-normal comparison in Fig. 4 we can easily eliminate the atop site as a possibility because of the poor agreement between the calculation and the [011] data. The atop model generates such a weak ARPEFS signal because there is no backscatterer near the photoemitter for this emission direction. The bridge site also bears some resemblance to the fourfold calculations for the same reason the atop model did in the normal emission comparison—the presence of a backscatterer. Thus, only the fourfold model compares favorably to the experimental curves in both emission directions.

2. Structural information

Once the site has been determined, MSSW calculations can be used to obtain structural details from the ARPEFS. We begin the quantitative extraction of the geometrical information by Fourier filtering the experimental results to eliminate high-frequency noise from the data; filtering also effectively reduces the cluster size necessary to model the fine structure by eliminating ARPEFS contributions from distant atoms. From the Fourier spectra of Figs. 2 and 3 we can estimate which are the structurally significant peaks and which are due to noise. For the normal emission data we inverse Fourier transformed the path-length difference spectrum, after zeroing out the intensity at distances larger than 15 Å, and we performed a similar transform for the [011] data after zeroing out data at path-length differences greater than 20 Å. All subsequent comparisons of theory to experiment were conducted with these filtered curves.

MSSW simulations were compared to the filtered data using a chi-squared-like procedure:[11]

$$r=\frac{\sum(\chi_{\text{expt}}-\chi_{\text{theory}})^2}{\sum\chi^2_{\text{expt}}}\ , \tag{4}$$

where χ_{expt} is the measured ARPEFS and χ_{theory} is a MSSW calculation with a fixed set of geometrical parameters. The structural parameters were varied beginning with the ones nearest the photoemitter, until an r-factor

minimum was found. The residual is useful in estimating the error associated with each structural parameter.[12] The denominator of r normalizes the residual, allowing a qualitative comparison amongst different emission directions and adsorbate systems. The structural parameters were varied in 0.1-Å increments for the initial assessment of the S/Cr(001) geometry; this reveals the coarse minima present in parameter space. In principle one might vary all structural parameters simultaneously in order to determine the absolute minimum, but this approach would be prohibitively expensive and time consuming. Instead, beginning with the unperturbed bulk structure of chromium and the geometrical results of Fourier analysis, the structural parameters were varied one or two at a time to optimize the geometry.

Figure 5 shows the two-dimensional projection of the residual surface generated by varying two parameters simultaneously. The center of each contour designates the r-factor minimum of varying two parameters: the sulfur- to first-layer chromium distance S-Cr(1) versus the sulfur- to second-layer chromium distance S-Cr^{atop} (2). The two contour diagrams of Fig. 5 clearly illustrate the directional sensitivity of ARPEFS. The normal emission fit exhibits a very steep curvature when varying the S-Cr(2) parameter and a much less severe gradient upon varying S-Cr(1). This indicates that the S-Cr(2) parameter is more sensitive than S-Cr(1) for the [001] data, which will be reflected in the estimated error for each of these parameters. The [011] off-normal fit shows greater sensitivity to the S-Cr(1) distance because in this emission geometry two first-layer Cr atoms are behind the photoemitter with respect to the emission direction. A similar conclusion was reached from the Fourier analysis.

The [011] emission direction was chosen for lateral sensitivity that could reveal corrugation of the Cr second layer. Because of the $c(2\times2)$ symmetry of the surface, only even (2, 4, 6, etc.) layers of the substrate have two symmetry-inequivalent atomic sites, thereby permitting corrugation. Odd-layer substrate atoms are identical by symmetry. In Fig. 6 we show the contours generated

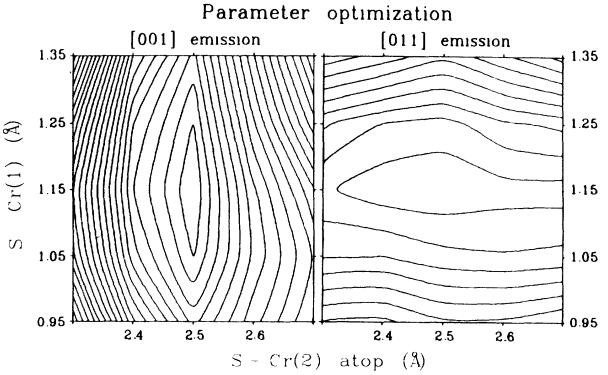

FIG. 5. Layer separation optimization: S-Cr(1) vs S-Cr^{atop}(2). Pictured are the two-dimensional projections of the residual surface generated by varying two structural parameters simultaneously. The r-factor value for the normal emission minimum is 0.14 and 0.32 for the [011] contour with a contour step increment of 0.1 for both.

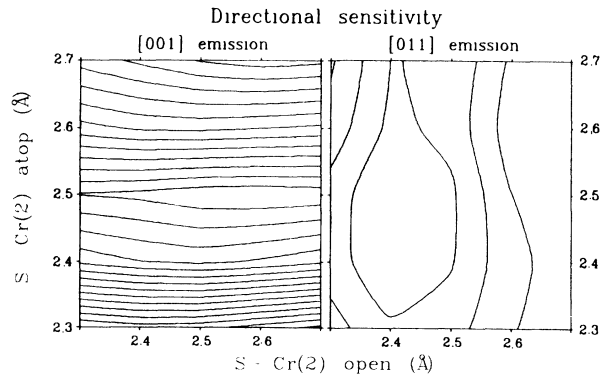

FIG. 6. Second layer substrate sensitivity: S-Cr^{atop}(2) vs S-Cr^{open}(2). These contours have the same step interval and minima as Fig. 5. The insensitivity of the normal direction to S-Cr^{open}(2) is evident by the lack of contour steps along that axis, while the [011] diagram shows several.

when optimizing the layer separation between sulfur and second-layer chromium with an adsorbate directly above S-Cr^{atop}(2) and S to second-layer Cr without an adsorbate above S-Cr^{open}(2). The normal emission data show great sensitivity to the S-Cr^{atop}(2) parameter, as would be expected, and great insensitivity to S-Cr^{open}(2). Figure 6 illustrates the [011] data's higher sensitivity to S-Cr^{open}(2). The relative insensitivity of the [011] data to S-Cr^{atop}(2) can be attributed to the Cr^{atop}(2) atoms lying near the nodal plane of the photoelectron p wave coming from the sulfur. Also the scattering angle for the second-layer Cr atom directly below the sulfur is 135° for the [011] direction. The scattering amplitude for this angle is quite low.

Once all geometrical parameters were determined, the emission direction was then optimized. In Sec. II, we estimated the precision of determining the emission geometry by laser autocollimation to be $\pm2°-3°$. A two-dimensional search around the nominal emission direction (by varying the polar and azimuthal angles) permitted the optimum direction to be found. MSSW calculations for different emission angles were compared to the experimental results indicating that the emission direction for the [001] data was 3° off normal. Likewise, the [011] emission data was found to be 3° from the nominal [011] direction. A similar procedure was carried out to optimize the photon polarization angle and uncertainties of $<3°$ were found. Once the optimized directions were determined, the structural parameters were reoptimized, and we found very little change in the values. Comparisons between the best fit MSSW calculation and experiment are shown in Fig. 7 for both emission directions.

The geometrical parameters that generated the optimum theory curves are listed in Table I. The Fourier transforms of each pair of comparisons are shown in Fig. 8, further illustrating the good fit. By comparing the theoretical Fourier transforms to the experimental transforms, constant-phase portions of the theoretical phase shifts that may be in error are partially eliminated, within a single-scattering context. This is evident in Eq. (2). The scattering phase shift ϕ_j contains some non-k-dependent part that causes a constant shift of the $\chi(k)$.

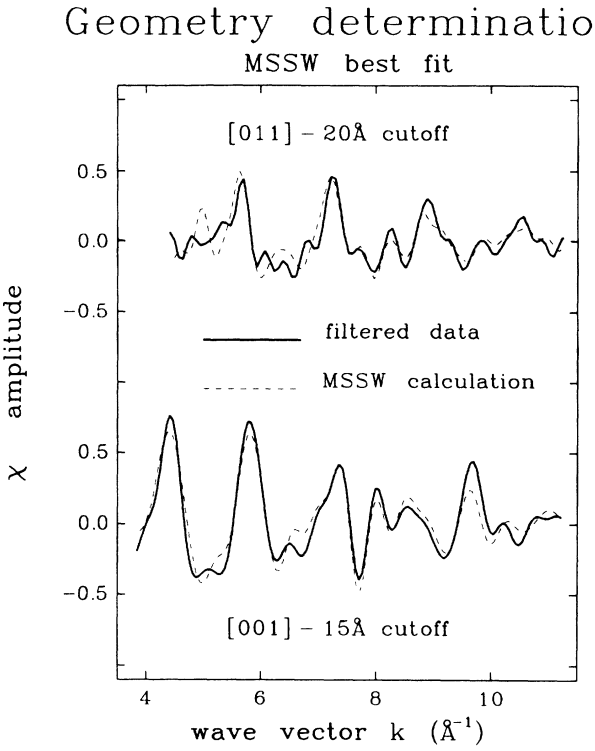

FIG. 7. Best-fit MSSW calculations compared to experimental curves. Each experimental curve (solid line) has been Fourier filtered and is compared to the MSSW calculated data (dashed line) that gives an absolute *r*-factor minimum. Structural parameters that generated the theory curves are listed in Table I.

However, this constant portion of the total phase, in both the theoretical and experimental data, will be absent in the transforms. Figure 8 also demonstrates that S/Cr(001) ARPEFS is sensitive to path lengths greater than 10 Å and that multiple-scattering spherical-wave analysis can model that near-surface information. Additional proof of the sensitivity of our data to long path-length difference scatterers is shown in Fig. 9. This figure shows that the high-frequency, long path-length information present in the photoemission fine structure is modeled by the MSSW simulation. MSSW calculations out to 10-Å path-length difference do not adequately model the high-frequency portions of the [011] data, while calculations out to 20 Å compare more favorably.

From Table I we find that the interlayer distance for S-Cr(1) is 1.17 Å and the S-Cr^{atop}(2) distance is 2.48 Å, giving a nominal Cr(1)-Cr(2) distance of 1.31 Å. This indicates that when sulfur is present in a $c(2\times2)$ overlayer on an otherwise clean Cr(001) surface the first two chromium layers *contract* approximately 8%. It is inconclusive as to whether the reconstruction is sulfur induced or not, because there are no clean Cr(001) quantitative surface structures with which to compare. Additional proof of contraction is observed when we calculate a MSSW $\chi(k)$ curve based on an unreconstructed geometry and compare it to experiment. Figure 10 shows such a comparison. In this diagram the theory curves are generated by retaining all the interlayer geometries determined from the multiple-scattering spherical-wave analysis except that the Cr(1)-Cr(2) distance is set to the bulk value of 1.44 Å. The normal emission comparison shows a great phase difference and is especially poor because of the strong S-Cr^{atop}(2) dependence of the [001] ARPEFS.

IV. DISCUSSION

Geometrical parameters obtained from the multiple-scattering analysis are summarized in Table I along with the error associated with each value. This error estimate was derived from the curvature of the *r* factors in Fig. 11, which were generated by varying one structural parameter at a time; this procedure of error analysis has been described elsewhere.[12] Our derived structural information and the error present in the experiment and analysis deserve commment. The errors associated with the [001] and [011] parameters in Table I do not reflect the true uncertainty of the value. Upon varying the surface or adsorbate Debye temperatures through physically reasonable values, the *r*-factor (reliability-factor) minimization procedure generates inconsistent minima for the structural parameters. The variation is not large (approximately 0.01 Å) but is associated with uncertainty in the nonstructural inputs to the analysis. The varying of other

TABLE I. Summary of the results obtained from MSSW analysis for each geometrical parameter. Parameter values for each emission direction correspond to *r*-factor minima with probable errors in last place (in parentheses) calculated from the *r*-factor curvature (Ref. 12). Adopted values represent the error-weighted average of the values from each emission direction. Distances in brackets are fairly insensitive parameters in the MSSW analysis and are reported to confirm the corresponding [001] results. Derived parameters are calculated from the adopted values.

Parameter	[001]	[011]	Adopted values	Derived values	
S-Cr(1)	1.165(60)	1.17(2)	1.17(2)	S—Cr(1) bond	2.35(1)
S-Cr^{atop}(2)	2.485(10)	2.465(60)	2.48(2)	Cr(1)—Cr(2)	1.31(2)
S-Cr^{open}(2)	2.585(90)	2.425(30)	2.44(3)		
S-Cr(3)	3.94(2)	3.97(3)	3.95(3)	Cr(2)—Cr(3)	1.47(3)
S-Cr^{atop}(4)	5.39(2)	[5.36(20)]	5.37(3)	Cr(3)—Cr(4)	1.42(3)
S-Cr^{open}(4)	5.38(5)	[5.42(11)]	5.39(5)		
S-Cr(5)	6.78(7)		6.78(7)	Cr(4)—Cr(5)	1.41(7)

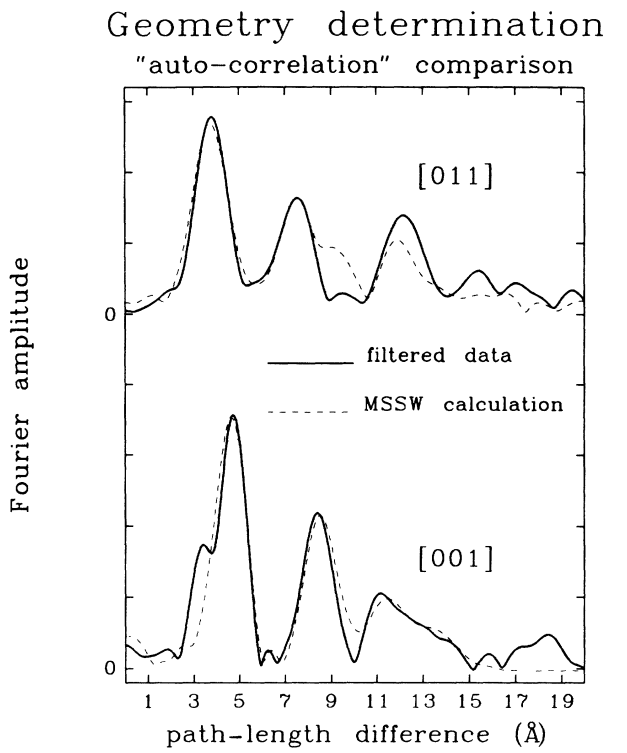

FIG. 8. Comparisons of experimental and calculated chi curves: Fourier transforms. Comparing the Fourier amplitudes of experimental (solid lines) and calculated (dashed lines) data for each of the emission directions illustrates the excellent agreement between theory and experiment. Constant phase errors in the theoretical phase shifts can be eliminated by comparing the Fourier spectra (see text).

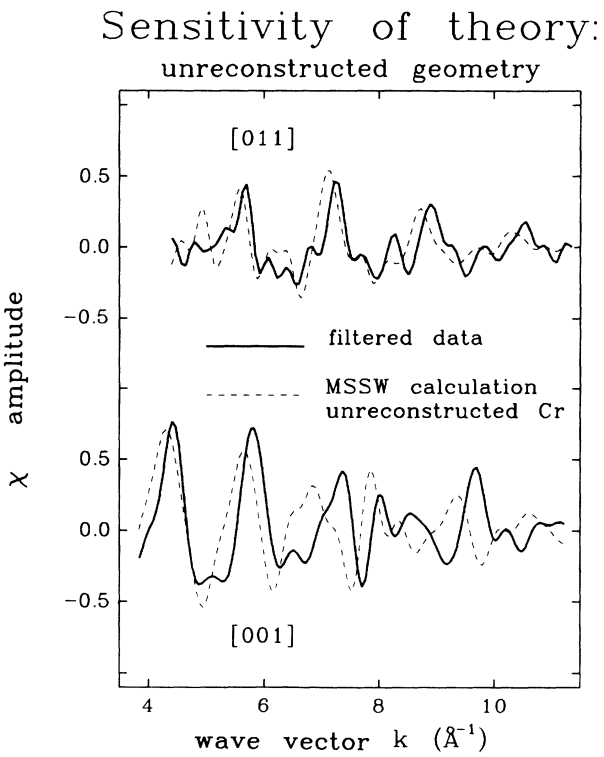

FIG. 10. Reconstruction sensitivity of ARPEFS. Filtered experimental data (solid line) compared to calculated results (dashed line) for each emission direction. Geometrical parameters for the theoretical curves are for an unreconstructed Cr(1)-Cr(2) separation. These poor fits show the sensitivity of ARPEFS upon going from the optimum Cr(1)-Cr(2) separation of 1.31 Å to the unreconstructed separation of 1.44 Å.

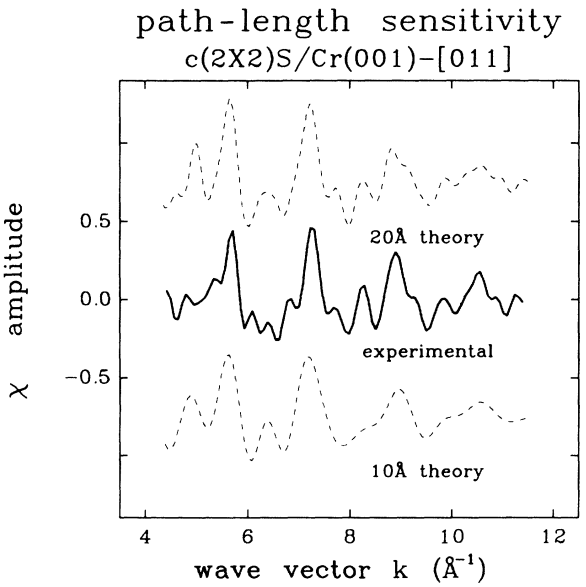

FIG. 9. ARPEFS path-length sensitivity beyond 10 Å. This compares the 20-Å filtered [011] data (solid line) to a MSSW curve calculated out to 10-Å path-length difference (lower dashed curve) and one calculated out to 20-Å scattering path length (upper dashed curve). The 20-Å calculated curve models the high-frequency structure of the data, while it is absent in the 10-Å one.

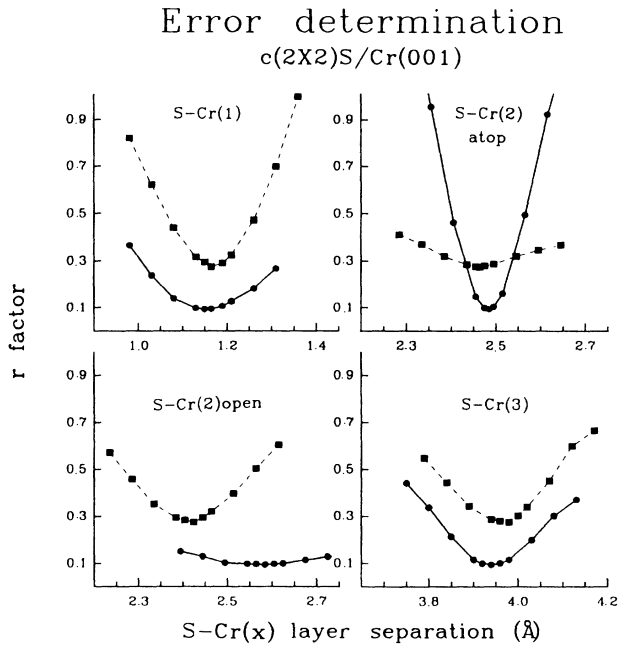

FIG. 11. Error determination from chi-square curvatures. Each panel shows the residual plots for the [001] (solid line) and [011] (dashed line) data. The absolute minimum for each curve is obtained by varying the labeled parameter keeping all others fixed. The error associated with each curve is determined by the curvature of the parabola.

nonstructural parameters generates similar fluctuations in the geometry, with the same degree of uncertainty.

For a truthful interpretation of the error, one must consider the geometry fluctuation caused by varying nonstructural parameters within physically reasonable limits, the statistical error inherent in the data, and the estimated error associated with our data reduction. Accounting for all these sources allows us to conclude that the best precision would be 0.02 Å for the most sensitive parameter, the S-$Cr^{atop}(2)$ distance. Estimates for other parameters are 0.02 Å for the S-Cr(1) distance and 0.03 Å for the S-Cr(3) and S-Cr(4) layer separations. These estimates compare favorably with earlier ARPEFS experiments and are expressed in Table I with the adopted values. Obviously, similar comments apply for SEXAFS-derived parameters.

It was noted earlier that the directional sensitivity of ARPEFS would allow us to examine any possible chromium second-layer corrugation. From Table I the adopted S-$Cr^{open}(2)$ value does show a slight shift (0.04 Å) towards the surface compared to $Cr^{atop}(2)$. This small shift is arguably within the error limit of the measurement, particularly when one considers the discrepancy between the [001] and [011] results for the S-$Cr^{open}(2)$ value. This discrepancy is illustrated in the lower left panel of Fig. 11 and in Fig. 6. The large difference between the [001] and [011] results for S-$Cr^{open}(2)$ can be attributed to the insensitivity of the normal emission data to this particular parameter. Based mostly on the [011] results, we can conclude that there is a slight 0.04-Å corrugation of the Cr second layer. The fourth layer shows greater consistency. The differences between the S-$Cr^{atop}(4)$ and S-$Cr^{open}(4)$ are within the error estimate for these parameters and allow us to conclude that there is no significant corrugation of this layer. The short-range surface effects do not penetrate deep into the bulk and rationalize why Cr(2)-Cr(3) and deeper layers essentially retain their bulk separation. An illustration of the chromium reconstruction, without second-layer corrugation, is shown in Fig. 12.

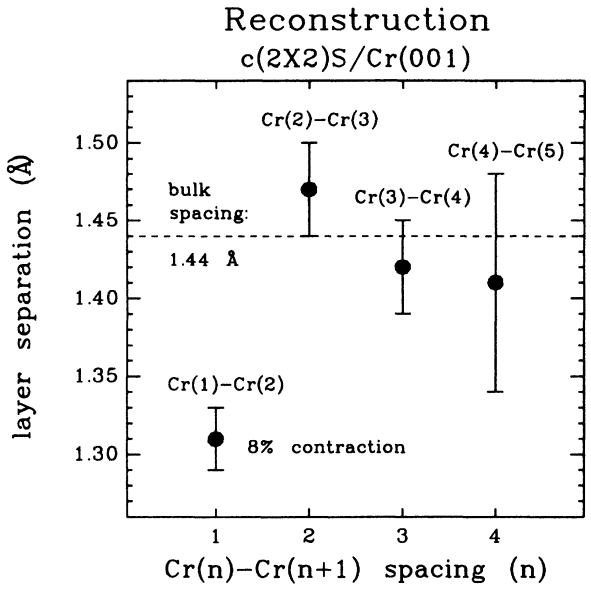

FIG. 12. c(2×2)S/Cr(001) contraction. The 8% contraction of the Cr(1)-Cr(2) layer separation to 1.31 Å and the slight expansion of Cr(2)-Cr(3). Deeper layers remain near bulk separations of 1.44 Å.

Theoretical phase shifts, surface MSRD, and mean-free-path values are among sources of error in the MSSW analysis that prompted our attempts to optimize some of these nonstructural parameters. Because the thermal averaging and inelastic dampening of the ARPEFS are difficult to distinguish from one another, it was inconclusive whether any anisotropy of the mean-square relative displacement existed. Temperature-dependant SEXAFS experiments have been used previously[36,35] to ascertain surface anisotropies in the MSRD, indicating that a similar temperature-dependant ARPEFS experiment would be ideal for such a study because of its directional sensitivity. Once a clearer description of surface MSRD anisotropies exists, other nonstructural values in the model can be better ascertained. Various values for the inner potential (V_0) were used, with $V_0 = 10.5$ eV giving the best fit between experiment and theory. Barton *et al.*[10] concluded that the uncertainty caused by these nongeometrical parameters is small and have little effect on the structural information.

Figure 8 illustrates another manifestation of nonstructural parameter uncertainty. The Fourier transform comparison of normal emission data to MSSW calculations shows a very good fit over the path-length range analyzed (up to 15 Å) except for the feature at 3.2 Å. This shoulder was assigned in Sec. III to scattering from the four nearest first-layer chromium atoms which have a normal emission scattering angle of approximately 120°. The simulated-data transform does not have a feature here and may be explained by the presence of a generalized Ramsauer-Townsend (GRT) resonance in the theoretical scattering factors, where for certain scattering angles the scattering amplitude goes to zero for a particular wave-vector value. This GRT effect has been observed in ARPEFS[38] and can manifest itself as the splitting of a Fourier feature. The experimentally determined scattering angle of 120° is very close to the angle of the GRT zeroing in the calculated scattering factors. This discrepancy between the [001] transforms of Fig. 8 may arise from scattering factor shortcomings that originate from inaccuracies in the scattering potentials and partial-wave phase shifts.

The difference between theory and experiment for the [011] data in Fig. 8 may well have similar origins. The presence of a feature in the theory at 9.2-Å path-length difference and its absence, or very low intensity, in the experimental data may also be caused by a GRT resonance. This path-length difference corresponds to scattering from a second-layer Cr atom directly below the photoemitter, through a scattering angle of 135°, which is near the GRT minimum. Interpretation of the discrepancies between theory and experiment should also consider that the analysis procedure may have generated these differences. A parallel experiment on c(2×2)S/Fe(001),[16] which bears many striking similari-

ties to our S/Cr(001) data because of a similar adsorption geometry, shows a Fourier peak in the [011] data near 9.2 Å. This suggests that the S/Cr 9.2-Å feature modeled by the MSSW theory may be real and that its absence or low intensity in the experiment may be caused by the analysis procedure itself. Alternatively, the theoretical scattering factor for Cr may be slightly in error—a plausible explanation given the sensitivity of GRT phenomenon to scattering angle. This would be an example of nonstructural parameters being the limiting factor.

Compared to other surface structures that have been obtained by ARPEFS, the 8% Cr(1)-Cr(2) contraction appears unusual. Such a contraction would be consistent with the S-Cr^{atop}(2) interaction being strong, thereby necessitating the reconstruction. This could arise from some sort of bonding interaction between the sulfur and second-layer Cr atom directly below it, not an unreasonable conclusion given the proximity (2.48 Å). Another possibility would involve the sulfur altering the electronic charge density within the first few layers of the chromium, thereby driving a steric change in the surface region. For example, withdrawal of electron density by sulfur could induce the Cr(1)-Cr(2) contraction by making the Cr atoms effectively smaller. A firm interpretation of reconstructions will require a better theoretical understanding of surface interactions and the nature of bonding on metals.

We have demonstrated that ARPEFS is sensitive to the third, fourth, and even fifth substrate layers, which show little or no change from the bulk layer separations (see Table I). The importance of near-surface structural information is twofold. First, the structural information itself is important. ARPEFS would be ideal as a probe of sandwich compounds because of its directional, surface, and chemical sensitivity and its newly demonstrated depth sensitivity. Second, this depth sensitivity would enable the fine tuning of many of the nonstructural surface parameters that were previously mentioned. By measuring surface MSRD anisotropies, one can compare them to bulk values. In general, various aspects of the surface region could be compared directly to those of the better-understood bulk within the same experiment.

V. CONCLUSIONS

Angle-resolved photoemission extended fine-structure measurements were made from the sulfur 1*s* core level on the $c(2\times2)$S/Cr(001) adsorbate system. We report the surface and near-surface structure of the system determined by two methods: Fourier analysis of the EXAFS-like oscillations which gives qualitative site and structure information and multiple-scattering spherical-wave analysis which gives more quantitative results. From our analysis the S-Cr(1) layer separation is determined to be 1.17 Å, giving a sulfur to chromium bond length of 2.35 Å. Our ARPEFS study also reveals a *contraction* of the first two chromium layers from the bulk value of 1.44 Å to 1.31 Å while corrugation was small in the second Cr layer and absent in the fourth layer. Deeper interlayer spacings remained at bulk values. By modeling the photoemission intensity with a Voigt function we attempted to eliminate one source of systematic error in the measurement. Including a Lorentzian contribution to the photopeak increased the total intensity thereby reducing the error associated with estimating the photopeak area.

From Fourier analysis the adsorption site was selected from three most reasonable possibilities: an atop, bridge, and fourfold site. By interpreting the peaks present in the Fourier transform with a single-scattering model of ARPEFS we were able to determine the geometry qualitatively. Our analysis also illustrated the sensitivity of ARPEFS to the near-surface region. The directional sensitivity of ARPEFS was exploited to uncover the subtle changes occurring at the chromium surface, and quantitative geometries were obtained by comparing the Fourier filtered experimental results with MSSW calculations. It has been previously shown[10,11] that multiple-scattering and spherical-wave considerations need to be included in order to obtain precise structural information. Structural parameters were optimized by performing an *r*-factor analysis between the experimental and theoretical curves and showed that for the S/Cr(001) case path-length differences greater than 10 Å were discernable and were successfully modeled by the MSSW calculations.

ACKNOWLEDGMENTS

One of the authors (L.J.T.) would like to thank J. J. Barton for helpful discussions and S. W. Robey for assistance with the phase-shift calculations. This work was supported by the Director, Office of Energy Research (Chemical Sciences Division of the Office of Basic Energy Sciences), U.S. Department of Energy under Contract No. DE-AC03-76SF0098. It was performed at the Stanford Synchrotron Radiation Laboratory, which is supported by the U.S. Department of Energy's Office of Basic Energy Sciences.

*Present address: Department of Physics, Zhejiang University, Hangzhou, Zhejiang, China.

†Present address: Department of Chemistry, University of Waterloo, Waterloo, Ontario, Canada N2L 3G1.

[1]A. Liebsch, Phys. Rev. Lett. **32**, 1203 (1974).

[2]A. Liebsch, Phys. Rev. B **13**, 544 (1976).

[3]S. Kono, C. S. Fadley, N. F. T. Hall, and Z. Hussain, Phys. Rev. Lett. **41**, 117 (1978).

[4]D. P. Woodruff, D. Norman, B. W. Holland, N. V. Smith, H. H. Farrell, and M. M. Traum, Phys. Rev. Lett. **41**, 1130 (1978).

[5]S. D. Kevan, D. H. Rosenblatt, D. Denley, B.-C. Lu, and D. A. Shirley, Phys. Rev. Lett. **41**, 1505 (1978).

[6]S. Y. Tong and C. H. Li, in *Chemistry and Physics of Solid Surfaces,* edited by R. Vanselow and W. England (Chemical Rubber Co., England, 1982), p. 287.

[7]Z. Hussain, D. A. Shirley, C. H. Li, and S. Y. Tong, Proc. Nat. Acad. Sci. U.S.A. **78**, 5293 (1981).

[8]J. J. Barton, C. C. Bahr, Z. Hussain, S. W. Robey, J. G. Tobin, L. E. Klebanoff, and D. A. Shirley, Phys. Rev. Lett. **51**, 272 (1983).
[9]P. J. Orders and C. S. Fadley, Phys. Rev. B **27**, 781 (1983).
[10]J. J. Barton, C. C. Bahr, S. W. Robey, Z. Hussain, E. Umbach, and D. A. Shirley, Phys. Rev. B **34**, 3807 (1986).
[11]S. W. Robey, J. J. Barton, C. C. Bahr, G. Liu, and D. A. Shirley, Phys. Rev. B **35**, 1108 (1987).
[12]C. C. Bahr, J. J. Barton, Z. Hussain, S. W. Robey, J. G. Tobin, and D. A. Shirley, Phys. Rev. B **35**, 3773 (1987).
[13]S. W. Robey, C. C. Bahr, Z. Hussain, J. J. Barton, K. T. Leung, Ji-ren Lou, A. E. Schach von Wittenau, and D. A. Shirley, Phys. Rev. B **35**, 5657 (1987).
[14]C. C. Bahr, S. W. Robey, Z. Hussain, L. J. Terminello, K. T. Leung, J.-R. Lou, A. E. Schach von Wittenau, and D. A. Shirley, Lawrence Berkeley Laboratory Report No. LBL-21221, 1986 (unpublished).
[15]J. J. Barton and D. A. Shirley, Phys. Rev. B **32**, 1892 (1985).
[16]X. S. Zhang, L. J. Terminello, S. Kim, Z. Q. Huang, A. E. Schach von Wittenau, and D. A. Shirley, Lawrence Berkeley Laboratory Report No. LBL-24248, 1988 (unpublished).
[17]A. G. Baca, L. E. Klebanoff, M. A. Schulz, E. Paparazzo, and D. A. Shirley, Surf. Sci. **171**, 255 (1986).
[18]G. Gewinner, J. C. Peruchetti, and A. Jaéglé, Surf. Sci. **122**, 383 (1982).
[19]L. E. Klebanoff, S. W. Robey, G. Liu, and D. A. Shirley, Phys. Rev. B **30**, 1048 (1984).
[20]L. E. Klebanoff, S. W. Robey, G. Liu, and D. A. Shirley, Phys. Rev. B **31**, 6379 (1985).
[21]J. S. Foord and R. M. Lambert, Surf. Sci. **115**, 141 (1982).
[22]A. G. Baca, L. E. Klebanoff, M. A. Schulz, E. Paparazzo, and D. A. Shirley, Surf. Sci. **173**, 215 (1986).
[23]J. S. Foord, A. P. C. Reed, and R. M. Lambert, Surf. Sci. **129**, 79 (1983).
[24]A. P. C. Reed, R. M. Lambert, and J. S. Foord, Surf. Sci. **134**, 689 (1983).
[25]Z. Hussain, E. Umbach, D. A. Shirley, J. Stöhr, and J. Feldhaus, Nucl. Instrum. Methods **195**, 115 (1982).
[26]S. D. Kevan, Ph.D. thesis, University of California, Berkeley, 1980.
[27]S. Doniach and M. Šunjić, J. Phys. C **3**, 285 (1970).
[28]J. Humlíček, J. Quant. Spectrosc. Radiat. Transfer **21**, 309 (1979).
[29]M. O. Krause and J. H. Oliver, J. Phys. Chem. Ref. Data **8**, 329 (1979).
[30]J. J. Barton and D. A. Shirley, Lawrence Berkeley Laboratory Report No. LBL-14758, 1985 (unpublished).
[31]E. O. Brigham, *The Fast Fourier Transform* (Prentice-Hall, Englewood Cliffs, NJ, 1974).
[32]J. J. Barton, S. W. Robey, and D. A. Shirley, Phys. Rev. B **34**, 778 (1986).
[33]J. B. Pendry, *Low Energy Electron Diffraction* (Academic, London, 1974).
[34]V. L. Moruzzi, J. F. Janak, and A. R. Williams, *Calculated Electronic Properties of Metals* (Pergamon, New York, 1978).
[35]P. Roubin, D. Chandesris, G. Rossi, J. Lecante, M. C. Desjongquères, and G. Tréglia, Phys. Rev. Lett. **56**, 1272 (1986).
[36]F. Sette, C. T. Chen, J. E. Rowe, and P. H. Citrin, Phys. Rev. Lett. **59**, 311 (1987).
[37]Geoffrey C. Allen, Philip M. Tucker, and Robert K. Wild, J. Chem. Soc. Faraday Trans. 2, **74**, 1126 (1978).
[38]J. J. Barton, Z. Hussain, and D. A. Shirley, Phys. Rev. B **35**, 933 (1987).